Interface Functionalities in Multilayer Stack Organic Light Emitting Transistors (OLETs)

Raffaella Capelli, Franco Dinelli, Massimo Gazzano, Riccardo D'Alpaos, Andrea Stefani, Gianluca Generali, Mauro Riva, Monica Montecchi, Angelo Giglia, and Luca Pasquali*

Herein is described a multidisciplinary approach to understand the performance limitations of small molecule organic light emitting transistors (OLETs) based on a layered architecture, an innovative architecture potentially competitive with the state of the art and more flexible for spectral emission control. The processes of charge injection and field-effect transport at metal/organic and organic/organic interfaces are analysed using microscopic and spectroscopic techniques in coordination. Atomic force microscopy and ultrasonic force microscopy are employed to characterize the interface morphology and the initial growth stages of organic films where charge transport actually occurs. X-ray diffraction and near edge X-ray dichroic absorption with linearly polarised light allow to determine the unit cell packing and the molecular orientation at the active organic interfaces, as well as the amount of non-ordered domains. Moreover, chemical reactivity at the interfaces is measured by X-ray photoelectron spectroscopy. It is found that a strong reaction occurs at the metal-organic interfaces, with molecular fragmentation. Additionally, the transport properties strongly depend on the nature of the materials forming the organic stack. Specifically, amorphous conjugated films as bottom layers can promote an increased molecular disorder in the upper active layer, with a concomitant deterioration of the conduction properties.

1. Introduction

Organic electronics and opto-electronics are playing a role ever more important as an alternative to silicon based technology. Plastic electronics can indeed open new opportunities for a relevant lowering of the production costs, as well as for a full disposability that silicon electronics cannot claim. Moreover, an appealing and innovative technology made of fully flexible and transparent devices can be naturally developed using organic materials. Plastic electronics can in principle support all the electronic and opto-electronic functions characteristic of silicon technology, starting from the basic integrated circuit elements up to light emission sources and energy generation, as is the case of photovoltaic cells.

In this emerging framework, many devices are based on an organic heterojunction to realise the active region for light generation and conversion. Typical examples are the organic light emitting diodes (OLEDs) and the planar (bulk) organic photovoltaic cells (OPVs). Recently, it has been demonstrated that also the most innovative devices can benefit from an heterojunction based active region. In particular, considering light emitting devices, efficient organic light emitting transistors (OLETs) have been successfully realized using a vertical multilayer architecture, with a higher degree of versatility with respect to the single layer OLET approach.[1–12] The single layer approach still represents the state of the art in terms of performances (brightness and external quantum efficiency (EQE)); however, the

Dr. R. Capelli, Dr. M. Montecchi, Dr. A. Giglia, Dr. L. Pasquali
CNR - Istituto Officina dei Materiali
S.S. 14, km 163.5 in Area Science Park
I-34012, Trieste, Italy
E-mail: capelli@iom.cnr.it
Dr. F. Dinelli
CNR- Istituto Nazionale di Ottica
Area della ricerca di Pisa - Via G. Moruzzi
1 Località S. Cataldo
56124, Pisa, Italy
Dr. M. Gazzano
CNR - Istituto per la Sintesi Organica e la Fotoreattività
via P. Gobetti 101 40129, Bologna, Italy
R. D'Alpaos, A. Stefani, Dr. G. Generali
ETC S.r.l. – Via P. Gobetti 101
40129, Bologna, Italy
Dr. M. Riva
SAES Getters S.P.A. – Viale Italia 77
20020, Lainate, MI, Italy
Dr. M. Montecchi, Dr. L. Pasquali
Dipartimento di Ingegneria 'Enzo Ferrari'
Università di Modena e Reggio Emilia
Via Vignolese 905 41125, Modena, Italy
Dr. L. Pasquali
Department of Physics
University of Johannesburg
PO Box 524
Auckland Park 2006, South Africa

DOI: 10.1002/adfm.201400877

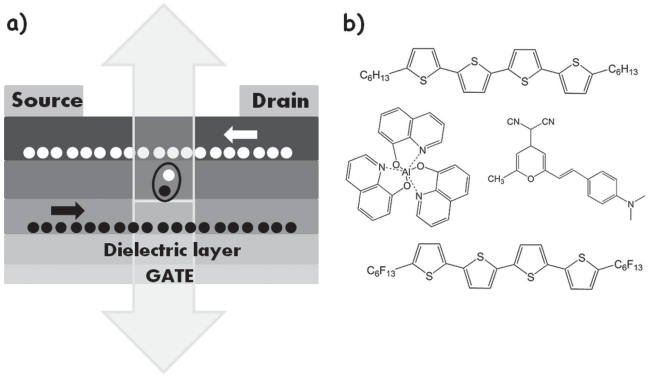

Figure 1. Scheme of a trilayer OLET reported in Ref. [6]. a) Device architecture and working principle. b) Molecular structure of the three layer compounds.

colour coordinate control would result much easier employing a multilayer OLET structure, moreover, multilayer based OLETs show a better ON/OFF ratio. In particular, in a well-balanced ambipolar single layer OLET representing the state of the art for EQE, the OFF state is not easy to define due to the minority charge carrier contribution at zero gate voltage. Also, it should be noticed that the state of the art EQE, reported for a single layer ambipolar OLET, corresponds to the minimum of the current circulating in the device.[11] Since the current is directly related to the number of excitons generated in the active region, this represents an intrinsic limitation in the total light power generation, not present in multilayer OLETs. For these reasons, the multilayer approach can play an important role in the development of the OLET technology, as it results closer to the applicative requirements.

Among the different multilayer OLET architectures, the trilayer stack one has gained a leading role. In this case, the organic stack consists of a superposition of a n-type and a p-type field-effect transport layers, separated by a recombination layer. In **Figure 1** the structure of the first reported trilayer OLET is sketched.[6] The n-type and p-type layers are made of conjugated molecules strongly interacting, that favour an ordered and oriented solid-state phase. The recombination region, instead, is an amorphous film of conjugated small molecules doped with highly emissive dyes. Trilayer OLET architectures can be also based on a fully polymeric or a mixed polymeric/oligomeric stack.

Good transport properties in both the bottom and the top layers have been demonstrated only for a particular OLET case.[10] More generally, instead, control of the transport properties within a trilayer stack has not been yet successfully achieved.[6,8,9] It is now consolidated that the physical properties of molecular thin films for organic electronics are mainly determined by the microscopic solid-state molecular packing. The charge transport properties originate from the intermolecular interaction of π-conjugated orbitals of neighbouring molecules. In this respect, within the frame of the hopping conduction model, the most relevant parameters are: the internal reorganization of the electronic energy levels (HOMO-LUMO) following the removal or the addiction of a charge; the unit cell packing of the molecular solid; the crystallinity degree of single-crystal domains; the average domain dimensions in the active region.[13–16]

In a vertical heterojunction architecture, sharp organic/organic interface regions in the multilayer stack play a central role in the determination of the molecular packing and relative molecular orientation. These may be no more controlled by the bulk intermolecular interaction, as is the case of a single material thin film, but the local interactions may become predominant. Moreover, a suitable interface engineering is fundamental for an effective exciton generation, at the basis of the light emission in the recombination layer, and for the field-effect charge transport occurring at the planar organic/organic interfaces between n- or p-transport layers and the recombination layer. In addition, the quality of organic/inorganic interfaces at metal contacts also appears a critical issue for an efficient charge injection.

The control and the understanding of the organic heterojunction formations and functionalities are thus very important. The aim of this paper is to address the morphological, structural and chemical properties of organic/organic and organic/metal interfaces in a layered system as used in a device, to understand their roles and , in perspective, to achieve a better control of the device performances. For this purpose we have therefore combined different microscopic and spectroscopic techniques, in order to obtain the largest amount of information.

2. Results and Discussion

Our present study is focused, in particular, to the investigation of the trilayer architecture proposed by Capelli et al. (Figure 1).[6] In this configuration, controlling of the field-effect transport properties of a top p-type layer has resulted particularly difficult. The first layer in contact with the dielectric is a n-type transport layer made of perfluorohexyl α,ω-disubstituted-quaterthiophene (DFH4T). The recombination region is formed by a host Alq3 matrix with a 1% 4-(dicyanomethylene)-2-methyl-6-(p-dimethylaminostyryl)-4H-pyran (DCM) dispersion. Finally, the top p-type transport layer is made of hexyl α,ω-disubstituted-quaterthiophene (DH4T), whereas the bottom dielectric is PMMA.

The energy level distribution of the reported tri-layer OLET heterojunction can be considered non-optimal for charge injection from the Au electrode into the organic active region. Indeed, if the energy barrier between the HOMO level of the hole transport layer (DH4T) and the Au work function (WF) is about 0.7 eV, the barrier for the electron injection from Au into the electron transport layer (DFH4T), through the DH4T/Alq_3 bi-layer, is even larger (about 2 eV). In spite of that, the n-type electrical characteristics of the tri-layer OLET show an almost ideal behaviour with a high mobility and a gate threshold value compatible with the use of a low k dielectric layer, as is the case of PMMA. On the other hand, an efficient charge injection via a tunnelling process has been demonstrated from Au to Alq_3, with an energy barrier of about 2 eV.[17] For this reasons, more than the non-optimal alignment of the energy levels between the organic stack and the metal electrodes, we believe that the poor hole transport of the top layer represents the main limitation affecting the performances of the tri-layer OLET reported in this work. This critical point might be related to the DH4T/Alq_3 interface but also to the Au/DH4T interface.

The impact of the interface roughness on the charge carriers percolation paths of an organic film is widely recognised.[18,19] In a stacked configuration, the roughness of the first deposited layer is often maintained in the second layer and even in the third layer. In the case of a DFH4T layer, a high RMS (root mean square) roughness value has been observed; sometimes it is even higher than 100 nm. Thus, the poor p-type mobility value could be due to either morphology or interfacial properties of the various films involved. To exclude the roughness issue, we have simplified the structure from tri to bilayers, by simply omitting the DFH4T layer from the OLET structure reported in ref.[6]. Therefore, we have restricted our experimental investigation to the Alq3/DH4T interface, comparing it to the PMMA/DH4T one.

The RMS roughness values for Alq3 and PMMA films are generally below 1 nm. Thus, we can consider them quasi-ideally flat surfaces. In **Figure 2** AFM images of the morphology of the pristine substrates and of DH4T films made of a fraction of a monolayer are reported. Figures 2a–2b refer to Glass/ITO/PMMA substrates, while Figures 2c– 2d refer to Glass/ITO/PMMA/Alq3(30 nm) ones. In particular, we can notice that the DH4T nucleation density is higher on PMMA (Figure 2b), with round shaped monolayer islands compared to the more irregular nuclei on Alq3 (Figure 2d). This is due to a lower mobility of the DH4T molecules on Alq3, suggesting stronger molecular interaction of the DH4T molecules with this surface. This is also suggested by Lateral Force data (not reported), showing larger friction on Alq3 regions. Once the first monolayer is complete, the shape of the islands nucleated in the second and upper monolayers is not anymore affected by the substrate. In **Figures 3**a–3b we report the morphology of 5 nm films grown on PMMA and Alq3. The islands on both substrates look similar in size and shape.

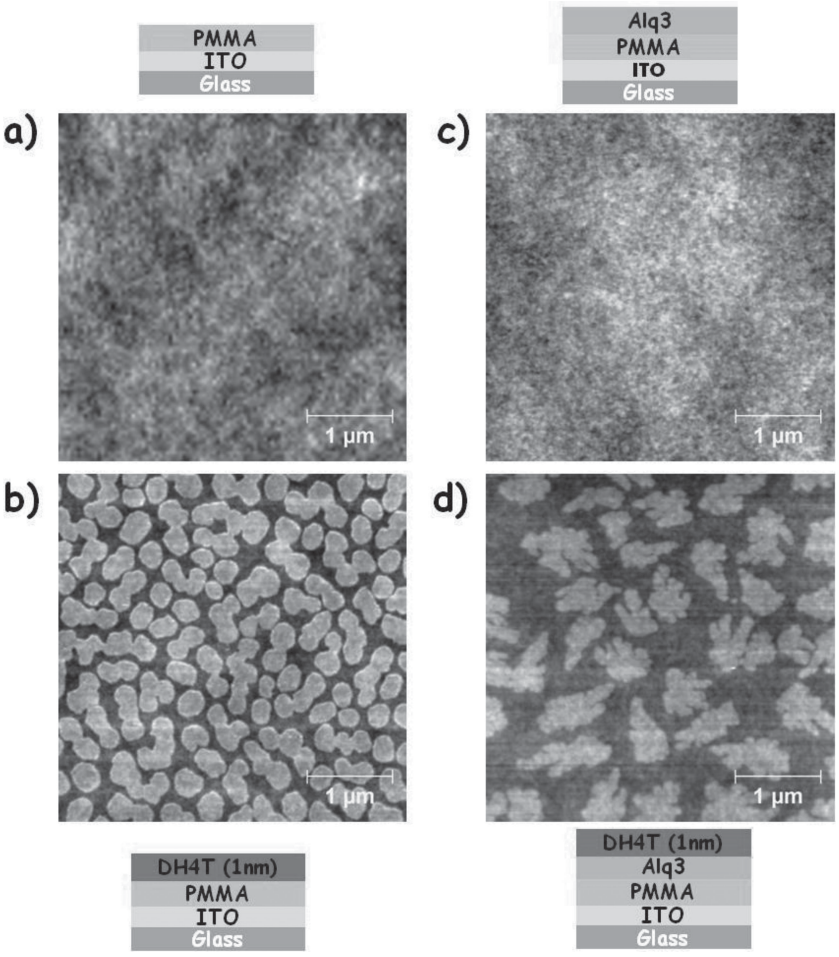

Figure 2. AFM images showing the topography of PMMA/DH4T and Alq3/DH4T bilayer structures: a) 300 nm thick pristine film of PMMA, b) 1 nm thick film of DH4T grown on pristine PMMA, c) 30 nm thick film of Alq3 on pristine PMMA, d) 1 nm thick film of DH4T grown on Alq3.

The electrical characteristics of DH4T based transistors (OTFT) grown, respectively, on PMMA and on the Alq3 film are reported in **Figure 4**. When the DH4T film is placed on top of Alq3, the field-effect transport properties result strongly degraded with respect to a film grown on PMMA. From these data it is clear that the interaction of the DH4T molecules with the Alq3 substrate introduces effects on the DH4T film transport properties that cannot be simply explained in terms of a large organic/organic interface roughness, as previously reported in Ref. [6].

Before discussing the electrical transport of DH4T in the Alq_3/DH4T bilayer structure, the contribution of the sole Alq_3 layer should be considered in order to clearly individuate its participation to the electrical transport of the whole system. The field-effect characteristics of a single layer Alq_3 FET are reported in the Supporting Information (see Figure S1). When Alq_3 is characterised in a transistor configuration, only a bulk charge transport is detected, with a maximum current intensity of ~10 nA. A gate modulation effect is completely absent. The multiple output curves are completely superimposed and the transfer curve is centred at about 12 nA, independently of the gate voltage. Since the Alq_3 based transistor is not modulated by the gate voltage, it is not possible to discriminate the type of charge carriers circulating in the device, electrons or holes. Being Alq_3 used as electron transport layer (ETL) in OLEDs, it is reasonable to assume that the charges at the origin of the device current are electrons. With reference to the results reported in Figure S1, a possible effect of Alq_3 in the Alq_3/DH4T bilayer transport could eventually appear as an increase of the sub-threshold current of the device, without affecting the field-effect part of the electrical curves. Moreover, in the Alq_3/DH4T device the charges are injected into the DH4T film, instead of being directly injected into the Alq_3 film (as is the case of Figure S1). For this reason the Alq_3 film is expected to have a negligible effect on the field-effect electrical characteristics of Alq_3/DH4T bilayer.

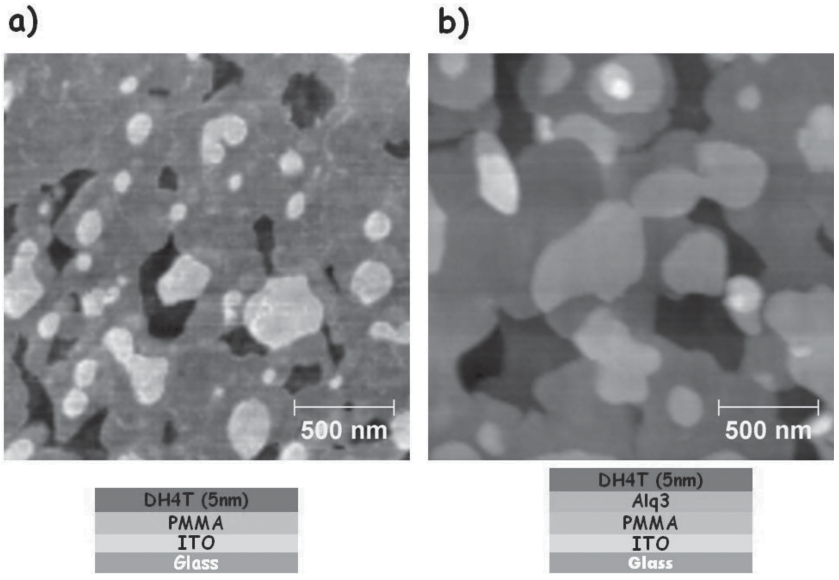

Figure 3. AFM images showing the topography of 5 nm thick films of DH4T grown on: a) PMMA; b) Alq3.

Additionally, the Alq_3 film could modify significantly the total capacitance acting on the DH4T film, with respect to the case of PMMA alone. This modification has been evaluated comparing the capacitances of ITO/PMMA/Au and ITO/PMMA/Alq_3/Au stacks. The results have excluded any relevant effect of the Alq_3 film on the device performances. In particular, no significant difference was detected with and without the Alq_3 film on top of the PMMA dielectric layer. On the other hand, the spin-coating process used to fabricate the 420 nm PMMA layer implies variations in the film thickness of up to 30 nm within the same total covered area, that cannot be avoided. Therefore, measurements of the PMMA capacitance taken in different regions of the substrate yield values of 7.0 ± 0.5 nF/cm^2. This range of values is fully compatible with the measurement performed by adding the 30 nm top Alq_3 film to the PMMA layer. In conclusion,

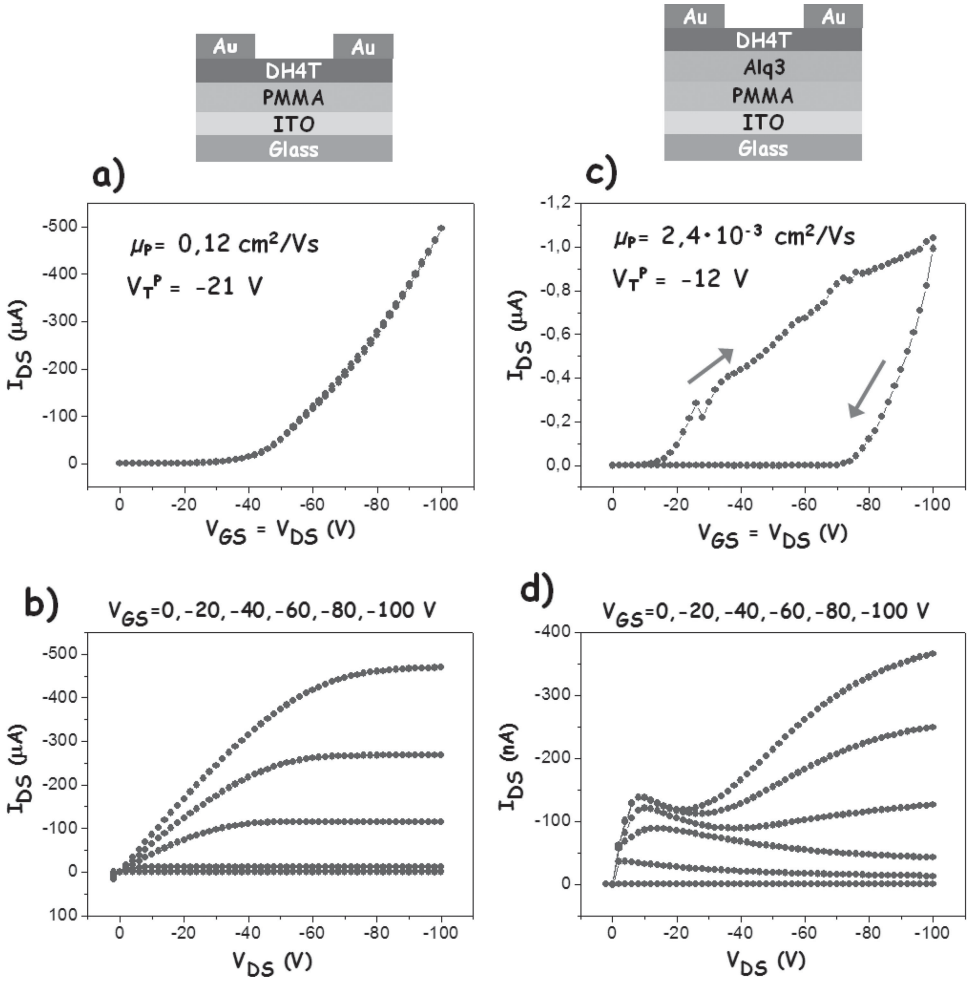

Figure 4. Electrical characteristics of DH4T based transistors. a) Locus curve with DH4T grown on top of PMMA. b) Output characteristics with DH4T grown on top of PMMA. c) Locus curve with DH4T grown on top of Alq3. d) Output characteristics with DH4T grown on top of Alq3.

the electrical role of Alq_3 can be considered negligible in discussing the DH4T field-effect characteristics, also for the Alq_3/DH4T bilayer configuration.

In particular, it is the field-effect mobility derived from the locus curve (Figures 4a, 4c) that results mostly affected by the presence of the interface with Alq3. In this case, the mobility is two orders of magnitude lower with respect to the DH4T/PMMA based device. The mobility and threshold here indicated are values extrapolated from the initial part of the forward locus curve, reported in Figure 4c, by using the standard MOSFET transistor mathematical description. Above a value of 25 V, a non-standard electrical behaviour characterizes the curve. The same mobility value can be extracted from the backward branch of the locus curve. In this case, the whole curve is consistent with a standard transistor description; the gate threshold voltage however results strongly increased (~ –70 V). In spite of a large hysteresis, the Alq3/DH4T transistor shows a lower current-on voltage with respect to the DH4T/PMMA one. With reference to Figure 4d, the field-effect current (I_{DS}) modulation of output curves follows a non-standard behaviour as a function of the drain-source applied voltage (V_{DS}). After an initial steep increase, I_{DS} appears to be limited in the V_{DS} range between -10 and –40 V, before reaching the saturation region. This effect, that prevents the standard linear dependence of I_{DS} on V_{DS}, as expected in the first part of the output curve, can be ascribed to a non-Ohmic contact behaviour, related to charge collection and injection taking place at the drain-source electrodes.[20,21] Low quality Au/DH4T interfaces, or traps located at the Au/DH4T interface, could also limit the total number of charge carriers flowing in the device, and this could be partially at the origin of a reduction in the current circulating within the DH4T OTFTs realized on top of Alq3, with respect to PMMA. As a macroscopic effect, this would imply a decrease in OTFT mobility. However, a two order of magnitude loss in charge mobility cannot be simply explained in terms of bad drain-source contacts alone. A role of the active transport layer must be invoked.

In addition to the effects described above, the electrical curves of Alq3/DH4T based OTFTs (Figure 4c) show a strong hysteresis that is absent in the PMMA case. This behaviour clearly indicates the presence of charge traps inside the DH4T film and in particular at the Alq3/DH4T interface, affecting mainly the device gate threshold.[22,23] Trapped charges at the Alq3/DH4T interface, indeed, tend to cancel the effect of the external applied gate voltage. As a consequence, the effective gate potential value applied to the mobile carriers within the DH4T film results lowered. We cannot exclude an active role of Alq3 molecules in trapping the holes flowing within the DH4T thin film, being the Alq3 HOMO positioned in an energy range very close to the DH4T HOMO, and being Alq3 a bulky electron-only transporter. In particular, the Alq_3 HOMO level is positioned at –5.7 eV, while the DH4T HOMO level is positioned at –5.8 eV.[24,25] The energy difference between the two states can be thus considered minimal. In summary, the mobility of DH4T OTFTs grown on Alq3 films might be affected by different phenomena, which cannot be discriminated by electrical measurements alone.

Deviations from the ideal field-effect behaviour have been observed by us on different devices based on amorphous-organic-layer/molecular-p-type-semiconductor stacks, where the amorphous-layer is made of conjugated molecules, as Alq3. In all cases mobility is reduced at least by two orders of magnitude and in most of them non-Ohmic injection is observed. As a representative example, in the SI we report the case of Pentacene on Alq3. In this particular configuration the relative positions of the HOMO levels in the bi-layer heterojunction does not favour the hole trapping at the interface in the bottom layer side. Since hysteresis seems not to be strongly affected by the level alignment, hole trapping in the bottom layer can be excluded as the cause of transport degradation.

Another possible cause of the bad performances could be represented by a degradation of the DH4T/Au interface occurring when DH4T is grown on top of Alq3. At the same time, the strong mobility decrease in the Alq3 based OTFTs suggests a possible change of the microscopic structure of the DH4T thin films. This may have as a consequence also the degradation of the DH4T/Au interface. In **Figure 5**a we show the morphology of a thin Au film grown on a thick DH4T film (15 nm on PMMA), obtained by AFM. The image in Figure 5b is obtained by simultaneously operating in Ultrasonic Force Mode (UFM). UFM allows one to characterize the elastic properties of the surface under analysis.[26,27] In this case, the UFM contrast is almost negligible, indicating that the 1 nm Au film has a homogeneous thickness. The shape of the DH4T islands below the Au film is not affected, excluding the presence of cracks that reflects the characteristic grainy structure of Au films. Thus we can assume that the DH4T film has not undergone a significant

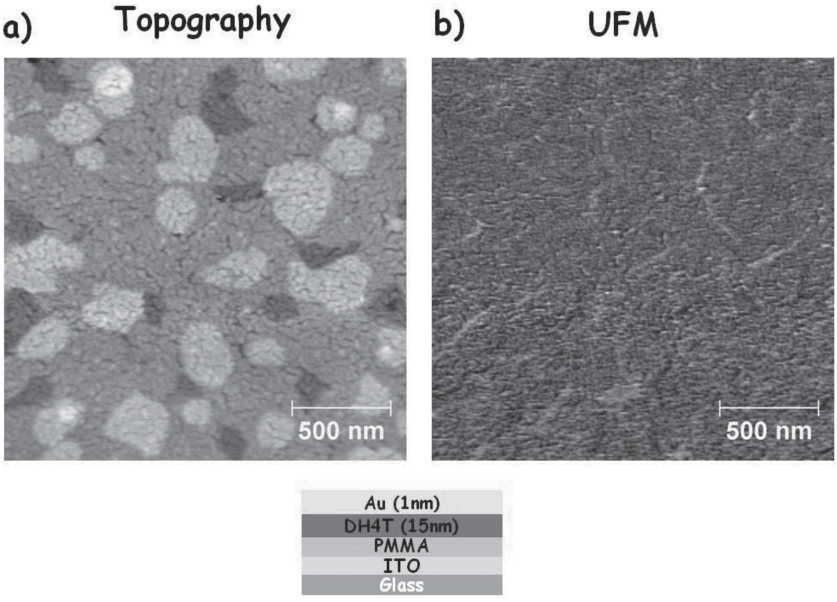

Figure 5. a) AFM image showing the topography of 1 nm thick film of Au grown on DH4T. b) UFM image of the same area, simultaneously acquired, showing the mechanical properties of the Au film.

damage (Figure 5a). However, this cannot be fully proven by considering only morphology. The DH4T molecules might have been damaged without losing their overall linear and rigid shape.

Another plausible reason for the DH4T thin film mobility impoverishment could be a change in the film molecular orientation with respect to the channel direction. This may also influence charge injection at the electrodes. In particular, if the DH4T molecules tilt in a way to orient themselves quasi-parallel to the substrate surface, the field-effect mobility can be strongly degraded. In this case, indeed, the conjugated inter-orbital overlap will extend in the vertical direction, instead of the horizontal direction that connects the drain and source electrodes. In such a way the charge transport will be vertically favoured and not horizontally as required. Another reason for the reduction in DH4T film mobility could be a rearrangement of the molecular packing within the film unit cell varying the inter-molecular distances, and thus the hopping integral. Finally, another issue related to the degradation of the DH4T thin film transport properties could be the degree of microscopic molecular order. In this case it is not a change in the unit cell structure that affects the film transport properties, but a broadening of the distribution width of the molecule positions and of the in-plane orientation of the ideal unit cell that may cause a transport degradation.

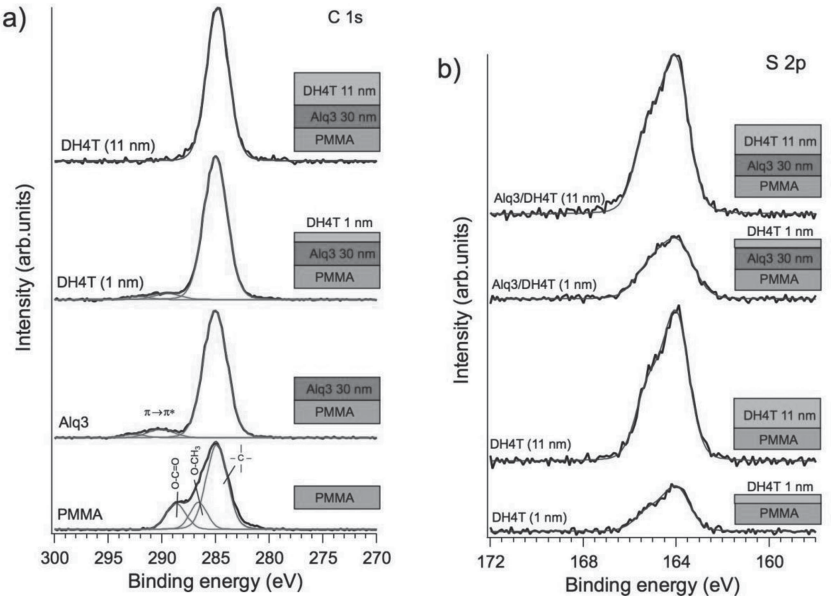

Figure 6. XPS spectra of PMMA/Alq3/DH4T trilayer. a) C 1s region taken at different deposition steps. b) S2p region for DH4T grown of PMMA and Alq3.

To investigate more in depth these phenomena, we have therefore combined different spectroscopic techniques in order to study the device interfaces mediating, from one side, the field-effect transport properties of the DH4T thin film and, from the other side, the charge injection process. We have focused our attention on the Alq3/DH4T and PMMA/DH4T interfaces, and on the DH4T/Au contact. Near edge X-ray absorption (NEXAFS) with linearly polarized light at the carbon K-edge has been employed to study the molecular orientation in the organic layer supporting the field-effect charge transport. PMMA/DH4T and Alq3/DH4T interfaces are compared with a DH4T film deposited on an Au evaporated substrate. Core level X-ray photoemission spectroscopy (XPS) has been also performed, to exclude possible chemical reaction taking place at the Alq3/DH4T or PMMA/DH4T interfaces, and to investigate the interaction between the DH4T molecules and the Au electrodes. We have additionally compared the results of angular dependent NEXAFS with X-ray diffraction (XRD) of DH4T films on PMMA and Alq3, respectively.

XPS has been performed on PMMA fresh substrates and at different stages of organic material deposition directly in situ. No trace of contamination can be observed at each different evaporation step. C1s spectra are shown in **Figure 6**a. PMMA presents three features, related to different carbon contributions in the polymer.[28] The spectrum deeply evolves after the evaporation of Alq3, showing a main large structure centred at about 285 eV and a broad satellite shoulder. The first structure can be associated to C-C, C-H, C-N and C-O components (the resolution does not allow us to distinguish each one, separately), while the shoulder at high binding energies is related to shake up effects.[29,30] DH4T basically presents a single broad peak at about 285 eV, superimposed to the main structure of Alq3, which is assigned to carbon atoms in the thiophene and to C-H in alkyl chains. It can be seen that increasing the DH4T layer thickness, the shake-up structure of Alq3 disappears and the peak FWHM sizably reduces from 2.5 eV (for Alq3) to 2.3 eV (11 nm DH4T). Together with the disappearance from XPS of Al2p, O1s and N1s peaks of Alq3 (not shown), this indicates that the DH4T layer is uniform and it does not present holes (see also morphology images). A similar picture is obtained when DH4T is evaporated directly on PMMA: PMMA features rapidly reduce in intensity with the overlayer growth, and only DH4T structures are observed for a thickness of about 10 nm (not shown).

S2p spectra taken on DH4T films deposited on PMMA and Alq3 are reported in Figure 6b. Spectra are fitted with Voight doublets, taking into account the S $2p_{3/2}$-$2p_{1/2}$ spin-orbit splitting of 1.2 eV. A unique doublet is observed in all spectra, with maximum of the 3/2 component at about 164 eV, which is assigned to S in bulk oligo-thiophene environment.[31,32] The situation is similar at high and low coverage for both type of substrates, suggesting no (chemical) interaction at the two organic/organic interfaces. To enhance the spectral resolution and better identify chemically reacted species, S2p spectra have been also acquired using synchrotron radiation. These are reported in **Figure 7**. A single well resolved doublet is now observed in Figure 7a for a 15 nm DH4T film on Au (taken in this case as the substrate, to avoid or reduce charging effects). This corresponds to S in oligo-thiophenes in bulk-like environment. A single doublet is also observed for a ultrathin film of DH4T on Alq3/Au (Figure 7b) although the peak Gaussian broadening passes from 0.6 eV for the 15 nm DH4T film (Figure 7a) to 1.0 eV for the 1 nm DH4Tfilm on Alq3 (Figure 7b). This may

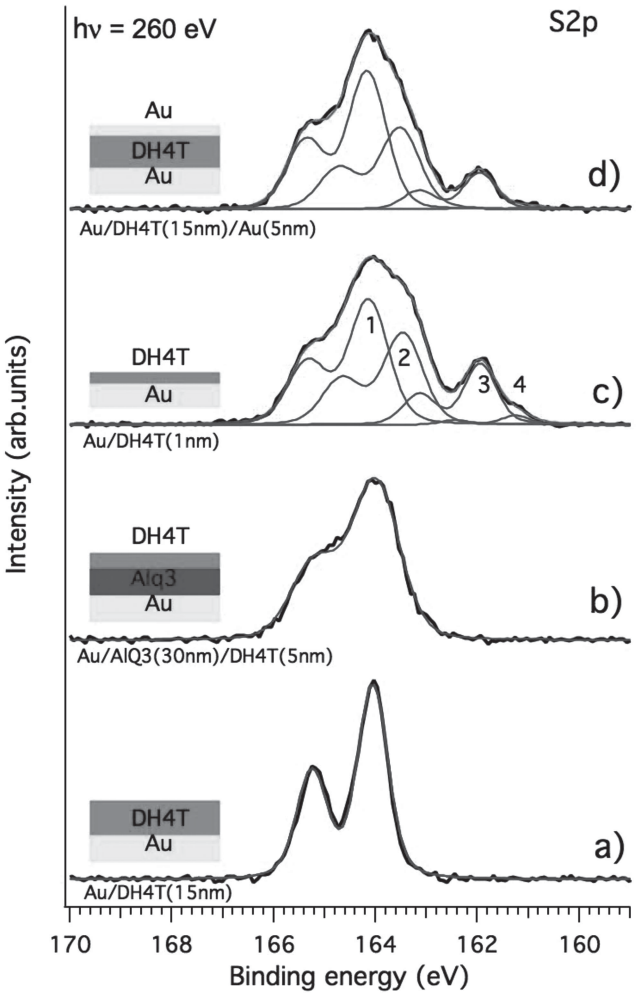

Figure 7. High resolution XPS spectra of Au/DH4T bilayer taken in correspondence of the S2p levels at normal emission.

be due to some level of sample charging, due to the Alq3 layer, worsening the overall resolution. This may also be related to molecular interaction at the interface between DH4T and Alq3, both conjugated molecules. In spite of this, spectra seem to exclude that a chemical interface reaction, chemical bonding or molecular dissociation, takes place between Alq3 and DH4T.

The situation is markedly different for the Au/DH4T interface. An ultrathin film of DH4T deposited onto a flat Au substrate shows multiple peak structures, which have been labelled from 1 to 4 (Figure 7c). Structure 1 is assigned to bulk thiophene species; feature 2 is related to thiophene rings at the close interface with Au, where the reduced binding energy is due to the enhanced screening of the photo-generated core hole by the substrate electronic charge. The additional low binding energy components 3 and 4 are associated to molecules reacting with Au. Similar effects have been already observed for other thiophene derivatives on Au.[33] In particular structure 3 is likely to be related to the formation of thiolate species, while feature 4 can be associated to some amount of atomic S or to differently bonding sites of the thiolates at the Au surface. It is noteworthy that the same reaction products are also observed if Au is deposited onto the DH4T film (Figure 7a). This is shown in Figure 7d when a nominal thickness of 5 nm of Au is deposited onto the organic material. In addition to chemical reaction, the interface is presumably highly diffused and intermixed, since a 5 nm thick Au layer would be largely sufficient to suppress any photoemission signal for the organic underlayer at the used photon energy (260 eV), if the Au layer was uniform and continuous.

These results clearly indicate that the interface is not inert with respect to chemical reactions and molecular dissociation takes place. For the first time this type of interaction between the organic semiconductor and the electrode has been observed in a realistic system. It is interesting to note that, looking to the electrical characteristics of DH4T based OTFT (Figures 4a, 4b) apparently there is no evidence of contact problems, being the curve shape almost ideal. Moreover, the AFM/UFM analysis doesn't show any indication of morphology variations at the DH4T/Au interface. In spite of that, the XPS spectra show the formation of an interface region made of Au intermixed with fragmented DH4T molecules. In light of that, the consolidated picture concerning the charge injection process at metal/organic interfaces could be partially reconsidered in its fundamental and technological aspects. In particular, the energy level alignment between the DH4T HOMO level and the Au work function is most likely affected by the existence of an intermixed region. Further investigation are needed in order to correlate the Au/DH4T interface energy level distribution to the chemical reactivity at that interface. We can expect that these features can have an influence on the performances of a device and should be taken into account in addition to the specific issues of the trilayer configuration. Moreover, we believe that this is a general feature of interfaces between thiophene derivatives and Au electrodes. These aspects should be carefully investigated, regarding their influence on a relevant class of organic devices. Molecular dissociation fragments could induce charge trapping at the electrodes. However, concerning the systems studied in this work, we would expect that the same chemical reactivity affecting the DH4T/Au interface of the single layer OTFT, shown in Figure 4a, would be equally present in the double layer OTFT, shown in Figure 4b. Therefore, this cannot be the sole cause at the origin of the different performances of the two devices.

As far as molecular orientation is concerned, NEXAFS has been performed at the C K edge for DH4T deposited on Au, Alq3 and PMMA. The DH4T films are sufficiently thick (about 10 nm) to mask the contributions from the substrate. Spectra acquired in s- and p geometries are shown in **Figure 8**, together with the corresponding difference curves. The Alq3 spectrum is shown in Figure 8a for comparison purposes. It is consistent with literature data and it will not be discussed further.[34] As expected it does not present any linear dichroism. DH4T presents pronounced resonances in the 285–289 eV region, which are mainly associated to the thiophene rings. In particular, the first main structure at 285.6 eV is associated to a C1sàπ^* transition, while the second feature peaked at 287.4 eV is assigned to a superposition of transitions to π^* states in the thiophene rings and to σ^* states due to C-S bonding.[33,35,36] σ^*(C–H) transitions in the alkyl side chains also contribute from 289 eV. Alkyl chains contribute also to the broad feature at about

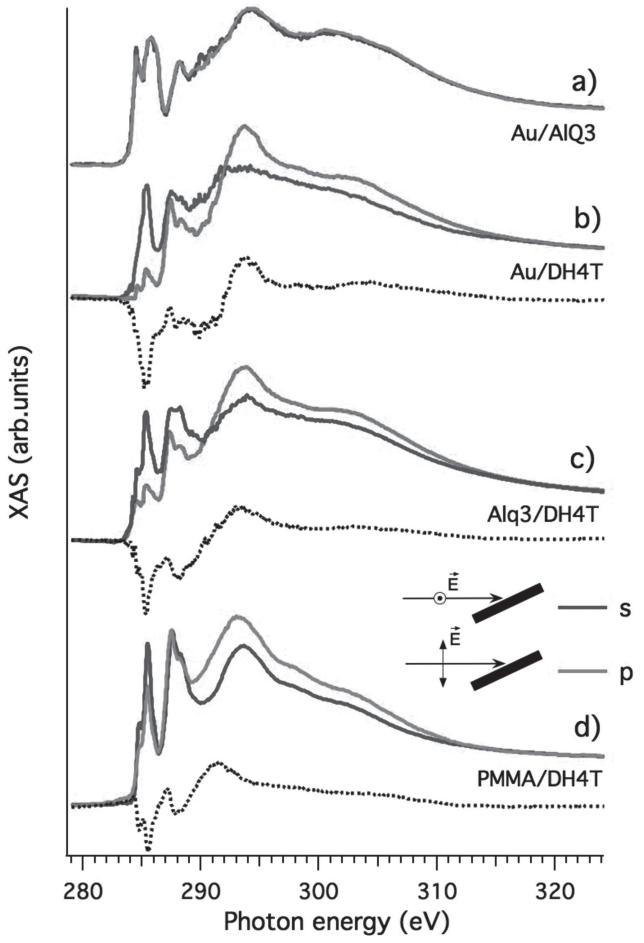

Figure 8. Dichroic NEXAFS spectra taken at the Carbon K-edge of DH4T films on different substrates. The spectrum of Alq3 is also shown.

294–295 eV, associated to σ^*(C–C) excitations, which are superimposed to analogous transitions in thiophene rings.

DH4T films deposited directly on Au (Figure 8b) present a strong linear dichroism. The behaviour of the first main structure, related to π^* transitions localised in the thiophene rings, indicates that the thiophene rings tend to adopt a vertical alignment. This is consistent with XRD data, as we shall discuss later. To derive quantitative information on the ring orientation relative to the substrate, we have applied the same procedure adopted in Ref.[37]. Taking into account the incidence angle conditions and beam polarization status, assuming that the film is isotropic in plane (due to randomly oriented domains parallel to the substrate plane), we obtain an average tilt angle of the thiophene ring planes of about 15° with respect to the substrate normal. When deposition is carried out directly on Alq3 (Figure 8c), the vertical alignment is still observed, although reduced, with a tilt angle of about 23°. This increases further to about 30° when the film is deposited on PMMA. These result point out that a slightly better vertical alignment is obtained on Alq3 than on PMMA.

The molecular alignment can affect the hopping integral and therefore the DH4T mobility value, as well as the charge carrier preferential transport direction.[13] In a first order approximation, the DH4T alignment impact on the hopping integral can be considered proportional to the difference between the DH4T inter-molecular distances for the two reported cases. We can roughly estimate this value as the Sine of the difference between the DH4T tilt angle values for the Alq3 and PMMA cases. This would give a difference of less than 2% and thus most probably negligible in the determination of the charge mobility values. Concerning the carriers preferential direction, in both cases the DH4T molecules are quasi-vertical so that the field-effect horizontal transport direction dominates.

In **Figures 9**a–9c the XRD data of DH4T layers (10 nm) grown on different substrates (Au/Alq3, PMMA/Alq3 and PMMA, respectively) are presented. The three patterns show the same peaks but with different intensities and widths. The peaks can be indexed on the basis of the DH4T crystal structure.[38] They belong to multiple orders of the same interplanar distance (d = 2.85 nm) revealing the organic material shows a strict orientation respect to the substrate. A very good simulation of the XRD pattern (Figure 9d) can be obtained assuming DH4T crystal domains with their *0 0 l* planes almost parallel to the substrate. This clearly indicates that the molecules are arranged as indicated in Figure 9f. The absence of appreciable reflections originating from other crystallographic planes, together with the intensity variations of all reflection peaks from sample to sample, which share the same thickness of 10 nm, suggest that a fraction of the thiophene molecules are in an amorphous state. The simulated pattern for a random distribution of ordered DH4T domains is shown in Figure 9f. Strong reflections are present at angular positions where the experimental diffraction patterns do not show any peak. This confirms that only amorphous DH4T phases, together with vertically aligned ordered molecular domains, are compatible with the experimental results. Random distribution of DH4T crystalline phases can be excluded. The intensity of the reflections increases as the substrate changes in the order Au/Alq3 < PMMA/Alq3 < PMMA. The highest amount of crystalline material is obtained on PMMA. The relative intensity of the reflections gives information on the orientation degree of the fraction of the ordered domains. It varies significantly in the order Au/Alq3 << PMMA/Alq3 ≈ PMMA. An evaluation of the dimension of the coherent crystalline domains can be done according to the Scherrer formula from the peak width in the direction perpendicular to the considered plane.[39] The average dimensions calculated from *0 0 2* peak are 12, 15, 17 ± 2 nm for Au/Alq3, Alq3 and PMMA, respectively. In summary, X-ray diffraction data indicate that the DH4T on PMMA results in a larger amount of ordered and oriented domains, with larger domain size with respect to the other substrates.

It should be noted that NEXAFS is a local probe, which is sensitive to the average orientation of the molecules. It is not strictly sensitive to the formation of ordered crystalline domains. This may explain the apparently conflicting pictures obtained from XRD and NEXAFS data. While on average, DH4T molecules seem to be more vertically aligned in sequence on Au, Alq3 and PMMA (Figure 8), the fraction of crystalline domains shows the inverse trend.

The physical picture emerging from the spectroscopic investigation of DH4T/PMMA and DH4T/PMMA interfaces is that a slightly better vertical molecular alignment can be obtained

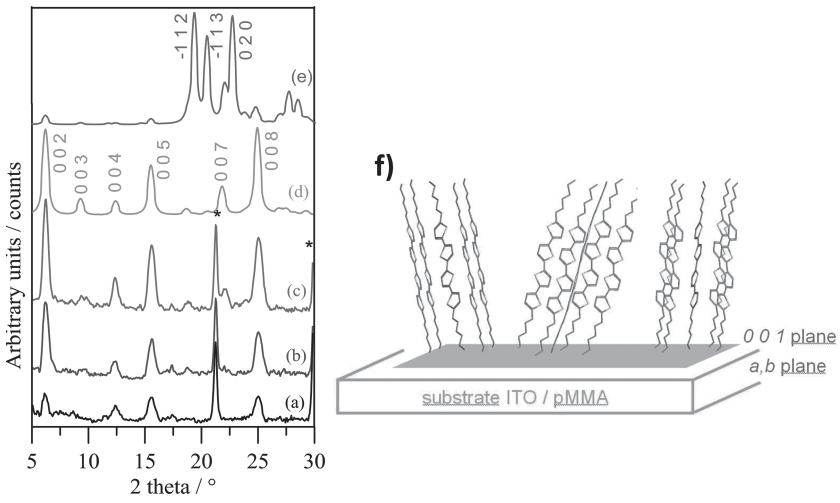

Figure 9. XRD patterns of DH4T layers grown on several substrates: a) Au/Alq3, b) PMMA/Alq3, c) PMMA. Calculated XRD patterns of DH4T: d) oriented with the crystallographic *ab* plane parallel to the substrate, e) randomly oriented. The peaks marked by an asterisk (*) are due to the ITO substrate. The Miller indexes of the main peaks are reported. f) A sketch of the molecular assembly of crystalline DH4T showing the position of the molecules respect to the substrate as deduced from the analysis of the XRD data.

when the DH4T film is grown on top of Alq3, but the differences with respect to PMMA are not sufficient to explain the differences in the OTFT behaviour. At the same time XRD characterization confirms the typical DH4T unit cell configuration for the DH4T film on top of PMMA, as well as on top of Alq3. On the other hand, an increase of the fraction of vertically aligned crystalline domains is observed for DH4T on PMMA. The reduction of the average size of crystalline domains inside the DH4T film on Alq3, at the expense of an increase of the amorphous regions, could be at the origin of the transport degradation. Moreover, the increasing extension of the disordered regions and/or the increasing density of the grain boundaries inside the DH4T films can be reasonably considered at the origin of the electrical hysteresis observed in the Alq_3/DH4T bi-layer structures. Defects in the molecular organization inside the DH4T films inevitably augment the amount of the electronic states that can act as charge traps and, as a consequence, a progressive increment of the population of these trap states originates the gradual shift of the gate threshold value.

The reason why crystallinity is reduced on Alq3, with respect to PMMA, is not yet fully understood. It is however possible to make some considerations and advance a hypothesis. DH4T films grown on conjugated crystalline films or amorphous non-conjugated polymeric films (PMMA) present generally good transport behaviour.[5] On the contrary, DH4T films grown on systems like Alq3, that is amorphous and conjugated, show similar poor performances. We can thus argue that, if both molecules in the films and in the substrate are conjugated, the interaction might increase. This interaction, combined with the amorphousness of the substrate, could contribute to increase disorder in the overlayer. This may also be consistent with the spectral broadening of the S2p peaks observed at the interface between DH4T and Alq3 with respect to bulk DH4T (Figure 7b). Further experimental work is needed to verify or disproof this hypothesis.

3. Conclusions

A multi-disciplinary investigation of Alq3/DH4T and DH4T/Au interfaces has been herein presented in order to better control the quality of the trilayer stack active regions in Organic Light Emitting Transistors (OLETs). Spectroscopic techniques, such as XRD, XPS, UPS and dichroic NEXAFS, have been combined with microscopic techniques, namely AFM and UFM, in order to obtain information on the molecular packing and the chemical reactivity of Alq3/DH4T and DH4T/Au interfaces. For the first time, we have been able to observe a clear chemical interaction between an organic semiconductor film and top electrodes of a real device. Thus, the DH4T molecular structure results damaged at the DH4T/Au interface due to a strong chemical interaction with Au. We can consider this as a general effect affecting all the organic devices based on thiophene derivatives.

On the other hand, no chemical reaction has been detected at the Alq3/DH4T interface. In particular, the DH4T unit cell packing as well as its mean molecular orientation are not affected by the presence of an Alq3 underlying layer. However, an increase in amorphousness has been observed with respect to DH4T films grown on PMMA. We cannot exclude that this increase in molecular disorder can also affect the quality of the DH4T/Au interface, altering the injection and collection of charge carriers. Ultimately, the decrease in crystallinity, observed in the presence of amorphous Alq3, can be considered the principal cause reducing the transport performances of DH4T films and thus at the origin of the non-optimal performances of OLETs based on a trilayer architecture.

4. Experimental Section

Organic thin film transistors are realised in a boom gate-top contact configuration. The channel length is 40 μm and the channel width 12 mm. A 420 nm thick film of PMMA, used as transistor dielectric, is spin-coated on top of a glass/ITO substrate and then annealed at 105 °C for 18 h. ITO being the common gate of a 8 transistor array. PMMA is purchased from ALL RESIST company. Thin organic films are grown by high vacuum sublimation in a Kurt J. Lesker commercial system. The base pressure is generally kept in the range 10^{-7}–10^{-6} mbar. The sublimation rate for the DH4T and Pentacene thin films is 0.1 Å/s, while for the Alq3 films is 2 Å/s. Au is grown at 1 Å/s. Alq3, and Pentacene powder are purchased from Sigma Aldrich at 99% purity degree and used as it is. DH4T molecules are provided by Polyera Corporation and used without additional purification. Electrical measurements are carried out by using a B1500A Agilent parameter analyser, contacting the sample trough a Suss PM5 probe station.

Thin films for in situ spectroscopic measurements are realised in the same conditions used for the device preparation, at a base pressure of 10^{-9} mbar. Conventional XPS is performed with a double pass cylindrical mirror analyzer (Perkin-Elmer PHI 15-255G cylindrical-mirror analyser) and MgKα photons (1253.6 eV) from a VG-XR3 double anode source, operated at 15 keV and 15 mA. The analyzer resolution is of 0.5 eV. High resolution XPS and NEXAFS spectra are acquired at the BEAR beamline

at the ELETTRA synchrotron radiation facility.[40,41] Absorption spectra are collected in total electron yield (TEY) mode (i.e. drain current mode) at the C K-edge with a resolution of 0.1 eV. Spectra are normalized to the incident photon flux and to the clean substrate signal. The incident beam is linearly polarized. The incidence angle of the light with respect to the sample surface plane is kept fixed at 8°, and the sample can be then rotated around the beam axis to change the polarization vector from *s* to *p* scattering geometry. Photoemission spectra at the S2p levels are taken at 260 eV of photon energy, to maximize surface sensitivity, with a hemispherical electron analyser (resolution of 0.1 eV).

The AFM employed is a prototype setup: the head is a commercial NT-MDT Smena; the electronics and the software used for control and acquisition are both developed in house. The tip used for this work is a standard silicon one (CSCS12, NT-MDT). Ultrasonic Force Microscopy (UFM) is operated at around 4 MHz with an amplitude modulation of less than 1 nm at around 4 kHz, by means of a piezo-plate located directly under the sample and driven by a function generator (Agilent 33220A).[26,27] Additionally, to collect the UFM data a digital lock-in amplifier (Zurich, HF2LI) is used. The color codes of the images are the following: topography, whiter for higher regions; UFM, whiter for higher elastic moduli.

The X-ray diffraction (XRD) analysis is carried out by means of a PANalytical X'Pert PRO powder diffractometer equipped with a Ni-filtered Cu Kα radiation and a fast X'Celerator detector. The data are collected in the 2θ range 5–30°, counting 1200 s at each step of 0.067°. The crystal sizes perpendicular to *0 0 2* planes are calculated by using the Scherrer method with the empirical form constant K = 0.94.

Supporting Information

Supporting Information is available from the Wiley Online Library or from the author.

Acknowledgements

The authors kindly acknowledge E.T.C. s.r.l for the research funding and the Institute for Nanostructured Materials of the Italian Research Council (CNR-ISMN) of Bologna for providing the fabrication and electrical characterization of devices at the basis of the work here reported. Part of the experiments were carried out in proposal 20120153 at ELETTRA.

Received: March 18, 2014
Revised: April 24, 2014
Published online: July 14, 2014

[1] A. Hepp, H. Heil, W. Weise, M. Ahles, R. Schmechel, H. von Seggern, *Phys. Rev. Lett.* **2003**, *91*, 157406.
[2] C. Santato, R. Capelli, M. A. Loi, M. Murgia, F. Cicoira, V. A. L. Roy, P. Stallinga, R. Zamboni, C. Rost, S. F. Karg, M. Muccini, *Synth. Metals* **2004**, *146*, 329.
[3] M. Muccini, *Nat. Mater.* **2006**, *5*, 605.
[4] C. Rost, S. Karg, W. Riess, M. A. Loi, M. Murgia, M. Muccini, *Appl. Phys. Lett.* **2004**, *85*, 1613.
[5] F. Dinelli, R. Capelli, M. A. Loi, M. Murgia, M. Muccini, A. Facchetti, T. J. Marks, *Adv. Mater.* **2006**, *18*, 1416.
[6] R. Capelli, S. Toffanin, G. Generali, H. Usta, A. Facchetti, M. Muccini, *Nat. Mater.* **2010**, *9*, 496.
[7] E. B. Namdas, P. Ledochowitsch, J. D. Yuen, D. Moses, A. J. Heeger, *Appl. Phys. Lett.* **2008**, *92*, 183304.
[8] E. B. Namdas, B. B. Y. Hsu, J. D. Yuen, I. D. W. Samuel, A. J. Heeger, *Adv. Mater.* **2011**, *23*, 2353.
[9] M. Ullah, K. Tandy, S. D. Yambem, M. Aljada, P. L. Burn, Paul Meredith, E. B. Namdas, *Adv. Mater.* **2013**, *25*, 6213.
[10] S. Toffanin, R. Capelli, W. Koopman, G. Generali, S. Cavallini, A. Stefani, D. Saguatti, G. Ruani, M. Muccini, *Laser Photon. Rev.* **2013**, *1*, 9.
[11] M. C. Gwinner, D. Kabra, M. Roberts, T. J. K. Brenner, B. H. Wallikewitz, C. R. McNeill, R. H. Friend, H. Sirringhaus, *Adv. Mater.* **2012**, *24*, 2728.
[12] M. Melucci, M. Zambianchi, L. Favaretto, M. Gazzano, A. Zanelli, M. Monari, R. Capelli, S. Troisi, S. Toffanind, M. Muccini, *Chem. Commun.* **2011**, *47*, 11840.
[13] A. Troisi, *Chem. Soc. Rev.* **2011**, *40*, 2347.
[14] H. Klauk, *Chem. Soc. Rev.* **2010**, *39*, 2643.
[15] A. Bolognesi, M. Berliocchi, M. Manenti, A. Di Carlo, P. Lugli, K. Lmimouni, C. Dufour, *IEEE Trans. Electron Devices* **2004**, *51*, 1997.
[16] S. D. Wang, T. Miyadera, T. Minari, Y. Aoyagi, K. Tsukagoshi, *Appl. Phys. Lett.* **2008**, *93*, 043311.
[17] T. Matsushima, C. Adachi, *Thin Solid Films* **2008**, *516*, 5069.
[18] S. Studel, S. De Vusser, S. De Jonge, D. Janssen, Stijn Verlaak, J. Genoe, Paul Heremans, *Appl. Phys. Lett.* **2004**, *85*, 4400.
[19] S. E. Fritz, T. W. Kelley, C. D. Frisbie, *J. Phys. Chem. B* **2005**, *109*, 10574.
[20] D. J. Gundlach, L. Zhou, J. A. Nichols, T. N. Jackson, P. V. Necliudovc, M. S. Shur, *J. Appl. Phys.* **2006**, *100*, 024509.
[21] D. J. Gundlach, L. L. Jia, T. N. Jackson, *IEEE Electron Device Letters* **2001**, *22*, 571.
[22] G. Gu, M. G. Kane, J. E. Doty, A. H. Firester, *Appl. Phys. Lett.* **2005**, *87*, 243512.
[23] F. R. Libsch, J. Kanicki, *Appl. Phys. Lett.* **1993**, *62*, 1286.
[24] R. H. Lee, Y. W. Huang, Y. Y. Wang, H. Y. Chang, *Thin Solid Films* **2008**, *516*, 5062.
[25] A. Facchetti, M. H. Yoon, C. L. Stern, G. R. Hutchison, M. A. Ratner, T. J. Marks, *J. Am. Chem. Soc.* **2004**, *126*, 13480.
[26] O. Kolosov, K. Yamanaka, *Jpn. J. Appl. Phys. 2-Lett.* **1993**, *32*, 1095.
[27] F. Dinelli, M. R. Castell, D. A. Ritchie, N. J. Mason, G. A. D. Briggs, O. V. Kolosov, *Phil. Mag. A* **2000**, *80*, 2299.
[28] S. W. Rosencrance, W. K. Way, N. Winograd, D. A. Shirley, *Surf. Sci. Spectra* **1993**, *2*, 71.
[29] T. W. Pi, H. H. Lee, H. H. Lin, J. Hwang, *J. Appl. Phys.* **2007**, *101*, 043704.
[30] F. Borgatti, I. Bergenti, F. Bona, V. Dediu, A. Fondacaro, S. Huotari, G. Monaco, D. A. MacLaren, J. N. Chapman, G. Panaccione, *Appl. Phys. Lett.* **2010**, *96*, 043306.
[31] F. Terzi, L. Pasquali, M. Montecchi, S. Nannarone, A. Viinikanoja, T. Aaritalo, M. Salomaki, J. Lukkari, B. P. Doyle, R. Seeber, *J. Phys. Chem. C* **2011**, *115*, 17836.
[32] E. O. Sako, H. Kondoh, I. Nakai, A. Nambu, T. Nakamura, T. Ohta, *Chem. Phys. Lett.* **2005**, *413*, 267.
[33] A. Nambu, H. Kondoh, I. Nakai, K. Amemiya, T. Ohta, *Surf. Sci.* **2003**, *530*, 101.
[34] A. Curioni, W. Andreoni, R. Treusch, F. J. Himpsel, E. Haskal, P. Seidler, C. Heske, S. Kakar, T. van Buuren, L. J. Terminello, *Appl. Phys. Lett.* **1998**, *72*, 1575.
[35] T. Okajima, S. Narioka, S. Tanimura, K. Hamano, T. Kurata, Y. Uehara, T. Araki, H. Ishii,Y. Ouchi, K. Seki, T. Ogama, H. Koezuka, *J. Electr. Spectr. Relat. Phenom.* **1996**, *78*, 379.
[36] L. Pasquali, Fabio Terzi, B. P. Doyle, R. Seeber, *J. Phys. Chem. C* **2012**, *116*, 15010.
[37] L. N. Serkovic Loli, H. Hamoudi, J. E. Gayone, M. L. Martiarena, E. A. Sanchez, O. Grizzi, L. Pasquali, S. Nannarone, B. P. Doyle, C. Dablemont, V. A. Esaulov, *J. Phys. Chem. C* **2009**, *113*, 17866.
[38] M. Moret, M. Campione, A. Borghesi, L. Miozzo, A. Sassella, S. Trabattoni, B. Lotz, A. Thierry, *J. Mater. Chem.* **2005**, *15*, 2444.

[39] H. P. Klug, L. E. Alexander *X-ray Diffraction Procedures for Polycrystalline and Amorphous Materials* 2nd ed., Wiley, New York, **1974**.
[40] S. Nannarone, F. Borgatti, A. Deluisa, B. P. Doyle, G. C. Gazzadi, A. Giglia, P. Finetti, N. Mahne, L. Pasquali, M. Pedio, G. Selvaggi, G. Naletto, M. G. Pelizzo, G. Tondello, *AIP Conf. Proc.* **2004**, *705*, 450.
[41] L. Pasquali, A. Deluisa, S. Nannarone, *AIP Conf. Proc.* **2004**, *705*, 1142.